Synthetic strategy for metallophthalocyanine covalent organic frameworks for electrochemical water oxidation

J J Jarju, A M Díez, L Frey, V Sousa, E Carbó-Argibay, L P L Gonçalves, D D Medina, O I Lebedev, Yu V Kolen'Ko, L M Salonen

Materials Today Chemistry 26 (2022) 101032

Contents lists available at ScienceDirect

Materials Today Chemistry

journal homepage: www.journals.elsevier.com/materials-today-chemistry/

Synthetic strategy for metallophthalocyanine covalent organic frameworks for electrochemical water oxidation

J.J. Jarju [a], A.M. Díez [a], L. Frey [b], V. Sousa [a], E. Carbó-Argibay [a], L.P.L. Gonçalves [a], D.D. Medina [b], O.I. Lebedev [c], Yu.V. Kolen'ko [a, *], L.M. Salonen [a, **]

[a] International Iberian Nanotechnology Laboratory, Avenida Mestre José Veiga, 4715-330, Braga, Portugal
[b] Department of Chemistry and Center for NanoScience (CeNS), Ludwig-Maximilians-University Munich (LMU), Butenandtstr. 5-11, D-81377, Munich, Germany
[c] Laboratoire CRISMAT, UMR 6508, CNRS-ENSICAEN, Caen 14050, France

ARTICLE INFO

Article history:
Received 1 April 2022
Received in revised form
3 June 2022
Accepted 5 June 2022
Available online xxx

Keywords:
Covalent organic frameworks
Phthalocyanines
Earth abundant transition metals
Electrocatalysis
Oxygen evolution reaction

ABSTRACT

Atomically dispersed metal catalysts are interesting materials for electrocatalysis. To this end, covalent organic frameworks (COFs) offer an excellent opportunity for the periodic placement of catalytically active single metal atoms within a porous framework. We report here a synthetic strategy to a series of imide-linked metal-containing phthalocyanine (Pc) COFs with different metal contents. Electrocatalytic activity of the materials towards oxygen evolution reaction was studied under alkaline conditions and the COF prepared from NiPc showed the best performance with current density $j = 10$ mA cm^{-2} being reached at overpotential $\eta_{10} \approx 410$ mV and Tafel slope of $b = 75$ mV/dec. In addition, the material showed excellent long-term stability during the testing time of 100 h.

1. Introduction

Atomically precise metal catalysts feature uniform active sites distributed throughout the material, thus bridging homogeneous and heterogeneous catalysts [1,2]. To this end, porous organic polymers (POPs) are interesting materials, as their porous nature can increase catalytic activity through enhanced accessibility of the active sites, and control of their composition and structure allows for the realization of catalyst materials with high precision at atomic level [3]. Among POP materials, covalent organic frameworks (COFs) are a class of crystalline, porous materials consisting of organic building blocks connected by covalent bonds [4,5]. Their structural regularity, tailorable nature through the introduction of functional molecules or moieties to the framework, and large surface area render them interesting materials for electrocatalysis [4,6–9], and, hence, COFs bearing metal-coordinating sites, such as bipyridine [10], salphen [11], or porphyrin [12], have been explored towards this application.

Phthalocyanines (Pcs) are rigid, chemically and thermally stable macrocyclic 18 π-electron aromatic compounds, the central cavity of which can be metallated to yield metallophthalocyanines (MPcs) [13]. These compounds are interesting materials for electrocatalysis due to the possibility of incorporating a wide variety of elements to the Pc core and their modifiable structure, which allows for precise tailoring of the catalytically active metal sites and synergy between them [14]. Consequently, MPc-containing materials have shown promising results as electrocatalysts for oxygen reduction reaction (ORR) [15], hydrogen evolution reaction (HER) [16], oxygen evolution reaction (OER) [14], CO_2 reduction reaction (CO_2RR) [17], and nitrogen reduction reaction (NRR) [18]. For example, Fe- and CoPc-based materials are promising platinum-group-metal-free catalysts for ORR [19]. Although some reports of MPc-containing COFs have emerged with high catalytic activities, for example towards CO_2RR [20,21] and recently also NRR [18,22], the limited number of synthetic strategies for MPc-containing COF materials hampers their wider exploration for electrocatalytic reactions.

Water electrolysis powered by renewable energy would provide a source for green hydrogen, and thus finding cheap and

* Corresponding author.
** Corresponding author
E-mail addresses: yury.kolenko@inl.int (Yu.V. Kolen'ko), laura.salonen@inl.int (L.M. Salonen).

https://doi.org/10.1016/j.mtchem.2022.101032

abundant alternatives to currently used expensive and rare platinum-group-metal electrocatalysts (Pt, RuO_2, IrO_2) is of utmost importance to allow for the scaling up of the water electrolysis technology [23–27]. To this end, earth-abundant transition-metal (TM) based catalysts show high promise under alkaline conditions for both HER and OER half-reactions of water electrolysis, with Ni- and NiFe-based materials representing the state of the art [28]. To allow for atomic dispersion of TMs within a porous organic framework, we were interested in realizing an MPc COF scaffold as platinum-group-metal-free material with electrocatalytic activity.

Herein, we report a synthetic strategy to a series of novel imide-linked MPc COFs with different TM loadings. Metal-free H_2Pc and metallated NiPc building blocks were prepared in three straightforward steps and used as starting materials for the crystallization of imide-linked COFs in ratios of 1:0, 1:1, and 0:1. Subsequently, Fe was incorporated to the prepared materials by post-synthetic metalation. Electrocatalytic activity of the newly synthesized COFs was measured towards OER under alkaline conditions, and NiPcCOF, with current densities j of 10, 50, and 100 mA cm^{-2} reached at overpotentials of 410 (η_{10}), 460 (η_{50}), and 510 (η_{100}) mV, respectively, showed catalytic activity among the best reported for Ni-bearing organic polymers. Moreover, the catalyst demonstrated stable performance during stability test, incurring a mere 0.5% loss in the applied potential over 100 h of sustained alkaline OER at the constant current density of 10 mA cm^{-2}. These performance metrics are a significant improvement over the values measured for metal-free H_2Pc, indicating that the imide-linked MPc COF scaffold is a credible electrocatalyst option for water oxidation using alkaline electrolyte.

2. Experimental section

2.1. Synthesis of Pc and MPc

H_2Pc [29,30] and NiPc [31] were synthesized following modified literature procedures (Scheme 1), for more details, see the Supplementary Material (SM).

2.2. Synthesis of COFs

2.2.1. General procedure for COF synthesis

COFs were prepared as presented in Scheme 2. MPc (0.07 mmol) and benzidine (0.14 mmol) were sonicated in *N*-methyl-2-pyrrolidone (NMP) (1 mL) and mesitylene (1 mL) in a 6 mL screw-capped Schott Duran culture tube for 10 min. Isoquinoline (0.1 mL) was added, the reaction mixture was sonicated for further 10 min, and heated at 200 °C for 5 days. The resultant solvothermal reaction mixture was cooled to room temperature, filtered, and washed with dimethyl sulfoxide (DMSO). Then, the product was washed with anhydrous DMSO in a capped glass vial in an oven at 60 °C overnight several times until the solvent was colorless. The product was collected by filtration, rinsed with acetone, soaked in acetone three times for 30 min, collected by filtration, and dried under nitrogen at 80 °C for 3 days to yield MPcCOF as black powder.

2.2.2. General procedure for post-synthetic metalation

$FeCl_2$ (100 equiv.) was dissolved in anhydrous dimethylformamide (DMF) (3 mL) in a 15 mL pressure tube, and the solution was degassed with N_2. MPcCOF (0.05 mmol) was added and the reaction mixture was heated in oil bath at 80 °C for 3 days. The reaction mixture was cooled to room temperature, filtered, and washed with methanol until the solvent was colorless. Then, the product was washed with anhydrous DMSO in a capped glass vial in an oven at 100 °C overnight several times until the solvent was colorless. The product was collected by filtration, rinsed with acetone, soaked in acetone three times for 30 min, collected by filtration, and dried under nitrogen at 80 °C for 3 days to yield Fe-containing MPcCOF as black powder.

2.3. Electrocatalysis

Alkaline OER properties of the synthesized materials were evaluated by the room temperature electrochemical measurement of cyclic voltammetry (CV) and chronopotentiometry (CP) using an Autolab PGSTAT302 N potentiostat/galvanostat (Metrohm), equipped with a FRA32 M frequency response analyzer (Metrohm) for

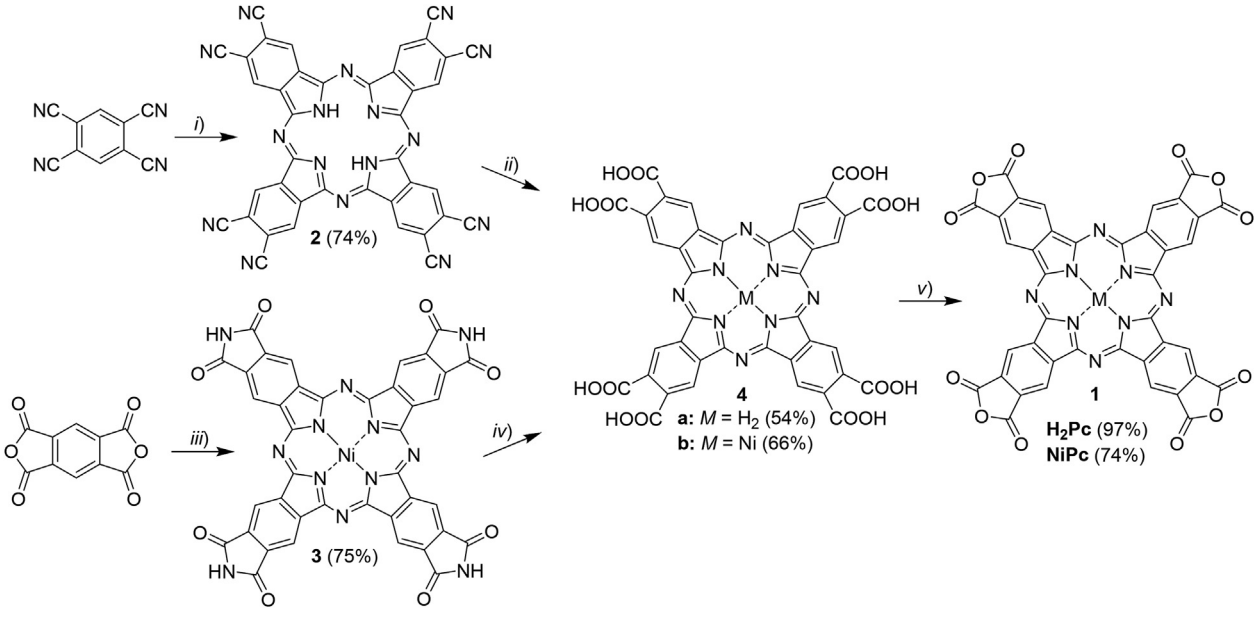

Scheme 1. Synthesis of H_2Pc and NiPc. Reaction conditions: i) Li, 1-propanol, 90 °C, 3 h; ii) KOH, triethylene glycol, 160 °C, 3 d; iii) urea, ammonium molybdate hexahydrate, $NiCl_2$, 250 °C, 5 h; iv) KOH, triethylene glycol, 160 °C, 20 h; and v) acetyl chloride, benzene, 90 °C, 24 h.

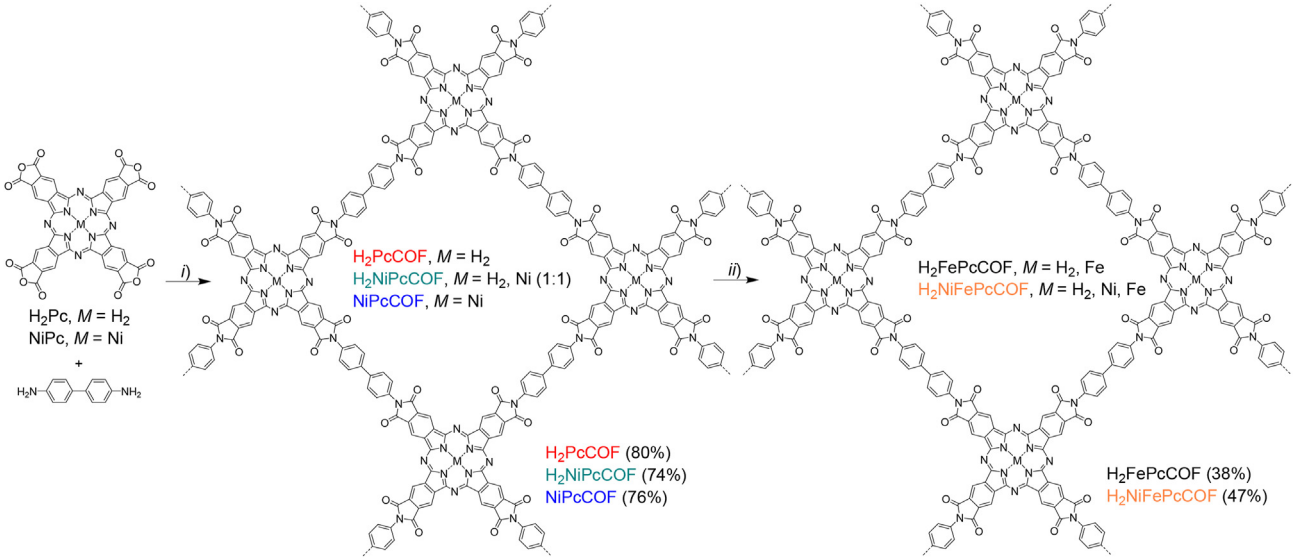

Scheme 2. Synthesis of the COFs from H_2Pc and NiPc and post-synthetic modification of H_2PcCOF and H_2NiPcCOF. Reaction conditions: *i*) mesitylene, NMP, isoquinoline (1:1:0.1), 200 °C, 5 d; *ii*) $FeCl_2$, DMF, 80 °C, 3 d.

electrochemical impedance spectroscopy (EIS). For the preparation of the working electrode (WE), the electrocatalyst (3 mg) was supported on 1 cm^2 Ni foam current collector (i.e., electrocatalyst mass loading per geometric area = 3 mg cm^{-2}) after having formulated the electrocatalytic ink (5 mg electrocatalyst, 50 μL Nafion ionomer, 1 mL ethanol), which was deposited dropwise (up to 640 μL) onto Ni foam. Pt wire was used as the counter electrode (CE) and calomel electrode as the reference electrode (RE). The experiments were carried out in purified Ar-saturated 1.0 M NaOH electrolyte.

3. Results

3.1. Synthesis

Tetraanhydride Pc **1** was chosen as the metal-containing building block due to the opportunity to obtain imide-linked COFs upon reaction with diamine linkers (Scheme 2). Such structures containing Co were recently reported to efficiently electrocatalyze CO_2 reduction [32]. Additionally, as compared to imine, the most commonly used linkage in COFs, imide COFs can feature higher stability under various conditions owing to the higher chemical stability of the imide linkage [33]. In addition, imide-based polymers can facilitate redox reactions, making them promising electrode materials [34].

We first prepared two tetraanhydride phthalocyanines, H_2Pc [29,30] and NiPc [31], through modified literature procedures (Scheme 1). The synthesis of H_2Pc started with the cyclotetramerization of 1,2,4,5-tetracyanobenzene to give 2,3,9,10,16,17,24,25-octakis(cyano)phthalocyanine **2** in 74% yield (Scheme 1). On the other hand, the first step of NiPc synthesis is the cyclotetramerization of pyromellitic anhydride and $NiCl_2$ to gain access to the corresponding tetraimide Ni phthalocyanine **3** in 75% yield. Thereafter, the products were converted to the corresponding 2,3,9,10,16,17,24,2-octakis(carboxy)phthalocyanines **4** under basic conditions, followed by decarboxylation with acetyl chloride to tetraanhydride derivatives H_2Pc and NiPc. The low solubility in organic solvents of both Pcs prevented their characterization by NMR spectroscopy; the compounds are only partially soluble in DMSO, NMP, and DMF. More information on the synthesis can be found in the SM.

To gain access to COFs with different degree of metalation, H_2Pc and NiPc in 1:0, 1:1, and 0:1 ratio were reacted with benzidine under solvothermal conditions using NMP and mesitylene as solvents and isoquinoline as catalyst in 1:1:0.1 ratio at 200 °C for 5 days (Scheme 2). H_2PcCOF (1:0 H_2Pc/NiPc), H_2NiPcCOF (1:1 H_2Pc/NiPc), and NiPcCOF (0:1 H_2Pc/NiPc) readily formed to give polyimide materials in 80%, 74%, and 76% yield, respectively. Subsequently, to incorporate Fe into the COFs, we carried out post-synthetic metalation by treating the as-synthesized H_2PcCOF and H_2NiPcCOF with a solution of $FeCl_2$ in DMF at 80 °C for 3 days. Thereby, H_2FeCOF and H_2NiFeCOF were obtained with moderate yields of 38% and 47%, respectively.

3.2. Structure

We then investigated the structure of the resultant COFs. Powder X-ray diffraction (XRD) confirmed the formation of crystalline precipitates of H_2PcCOF, H_2NiPcCOF, and NiPcCOF (Fig. S1–S3). H_2PcCOF shows four main reflections at 2θ = 3.9, 6.6, 9.9, and 27.5° (Fig. 1a). Four main XRD reflections were also observed for H_2NiPcCOF at 2θ = 3.8, 6.6, 10.0, and 27.6°, and for NiPcCOF at 2θ = 3.3, 7.1, 10.2, and 27.5°. As side product, a minor amount of NiO was detected by the XRD in the NiPcCOF sample (Fig. S3), which could stem from oxidation of either leached Ni from the Pc core during the COF synthesis or minor Ni-containing impurities in the NiPc building block. Structure models were constructed using the Materials Studio software package (Accelrys Inc.), the structure simulations and geometry optimization were carried out using the Forcite module employing the universal force field and *P*1 symmetry; for the estimated unit cell parameters, see Table S1 in the SM.

H_2FePcCOF retained its crystallinity during post-metalation and four main reflections were found at 2θ = 3.9, 6.6, 9.9, and 27.5° (Fig. 1d and S4). For H_2NiFePcCOF, however, the long-range order was lost, and three broad reflections were found at 2θ = 3.5, 10.0, and 27.5°. In addition, the formation of Fe_2O_3 as side product of the post-metalation of H_2NiFePcCOF was detected by the XRD (Fig. S5).

We next sought to study the chemical bonding in the as-synthesized COFs. The formation of the imide bonds was confirmed by Fourier-transform infrared spectroscopy (FTIR), where the spectra showed signals at 1771 and 1716 cm^{-1} for

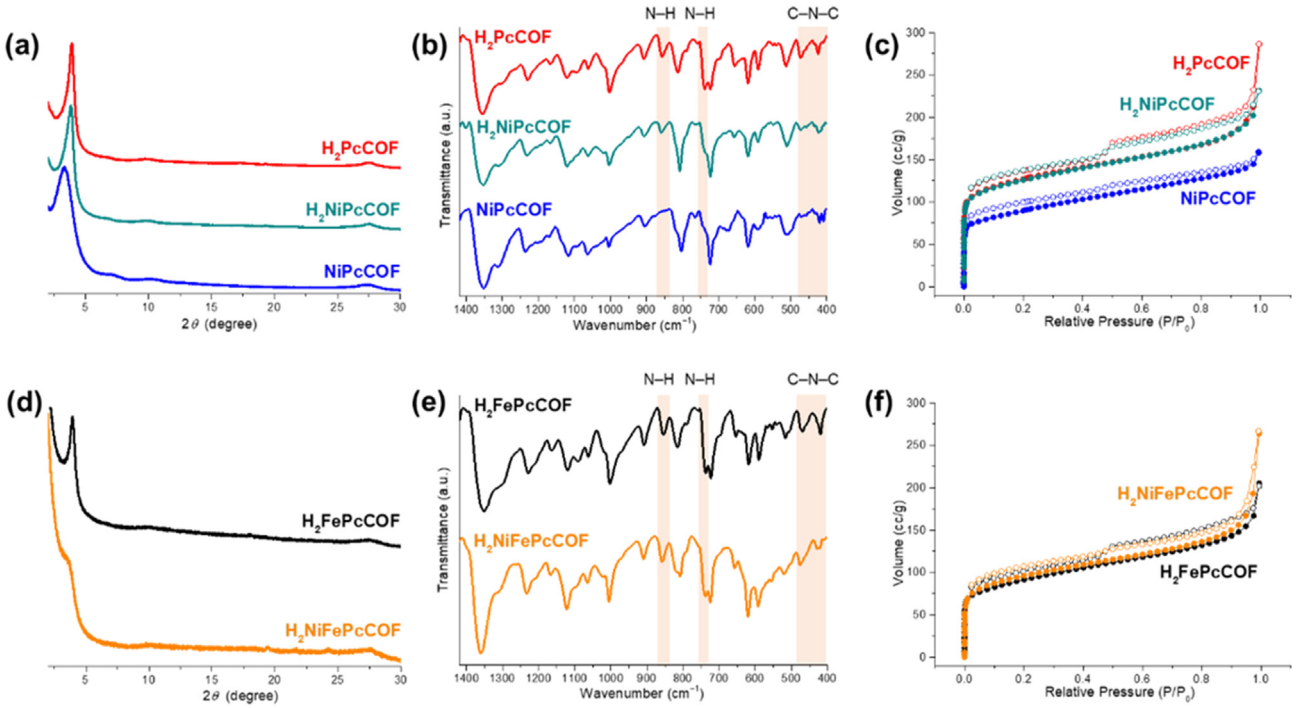

Fig. 1. (a,d) XRD patterns, (b,e) FTIR at wavenumbers 1420–400 cm^{-1}, and (c,f) N_2 physisorption isotherms at 77 K of H_2PcCOF, H_2NiPcCOF, NiPcCOF, H_2FePcCOF, and H_2NiFePcCOF.

H_2PcCOF, H_2NiPcCOF, NiPcCOF, and H_2FePcCOF, as well as at 1774 and 1720 cm^{-1} for H_2NiFePcCOF, attributed to the C= O moieties (Fig. 1b,e). The signals at 1355 cm^{-1} for H_2PcCOF, 1352 cm^{-1} for H_2NiPcCOF, 1349 cm^{-1} for NiPcCOF, 1351 cm^{-1} for H_2FePcCOF, and 1359 cm^{-1} for H_2NiFePcCOF were attributed to the C–N stretching of the imide (Fig. 1b,e and S6–S8 and Table S2).

Notably, the absence of both primary amine N–H stretching at ≈3350 cm^{-1} from benzidine and anhydride C= O stretching at ≈1840 cm^{-1} of the MPc starting materials also confirmed the success of the reaction (Fig. S7). In the case of NiPcCOF, the absence of the signals corresponding to N–H out-of-plane bending at ≈857 cm^{-1} and N–H wagging at ≈739 cm^{-1} indicated that the Pc cavity is occupied by the metal. In addition, differences in the signals for C–N–C bending at 400–500 cm^{-1} between the metal-containing COFs and H_2PcCOF (Fig. 1b) indicate complexation of Ni to the Pc cavity.

3.3. Textural properties

We next carried out nitrogen physisorption measurements at 77 K to investigate the textural properties of the COFs (Table S3). The results showed type I isotherms, with Brunauer–Emmett–Teller surface areas S_{BET} of 467, 462, 323, 326, and 346 m^2/g obtained for H_2PcCOF, H_2NiPcCOF, NiPcCOF, H_2FePcCOF, and H_2NiFePcCOF, respectively (Fig. 1c and S9–S18). The pore size distribution calculated using the quenched-solid density functional theory (QSDFT) adsorption branch model for cylindrical pores revealed pore diameter of 1.2 nm for H_2PcCOF, 1.3 nm for H_2NiPcCOF and H_2FePcCOF, and 1.4 nm for NiPcCOF and H_2NiFePcCOF (Fig. S9–S18), as well as a contribution of mesopores.

3.4. Microstructure and composition

Next, we used electron microscopy to study the microstructure and chemical composition of the synthesized COF materials. Scanning electron microscopy (SEM) images evidenced that the materials featured an irregular granular morphology (Fig. S19). In the case of NiPcCOF, SEM showed spherical morphology (Fig. 2a and b), which was also seen in the high-angle annular dark-field scanning transmission electron microscopy (HAADF–STEM) images (Fig. 2c and d). Energy-dispersive X-ray spectroscopy elemental mapping in STEM mode (STEM–EDX) confirmed the homogeneous distribution of O, C, and Ni throughout the material (Fig. 2e). Although some content of inorganic material was observed by HAADF–STEM analysis, presumably NiO as evidenced by XRD, the COF content was qualitatively confirmed to account for the majority of the as-synthesized NiPcCOF material. Furthermore, we analyzed NiPcCOF using X-ray photoelectron spectroscopy (XPS), and the spectrum demonstrated the presence of Ni, O, N, and C elements (Fig. S20 a). The high-resolution Ni 2*p* spectrum indicated the existence of Ni^{2+} with the presence of two peaks at 855.1 eV (Ni $2p_{3/2}$) and at 872.4 eV (Ni $2p_{1/2}$) and the respective satellite peaks, in accordance with that reported for polymeric NiPc material [35].

Metal content of the prepared materials was measured using inductively coupled plasma–optical emission spectrometry (ICP–OES). Ni content of 5.1% and 2.4% was found for H_2NiPcCOF and NiPcCOF, respectively, which is in excellent agreement with the theoretically expected values (5.1% and 2.6%), thus indicating that little to no de-metalation of MPcs occurred during the synthesis. H_2FeCOF was found to contain 2.1% of Fe (theor. 4.9%), suggesting that around 40% of the Pcs were metallated with Fe. For H_2NiFeCOF, Ni and Fe content of 1.8% and 5.2% were found (theor. 2.6% and 2.4% for COF with 1:1 NiPc/FePc), respectively. Hence, a third of the Ni leached during post-metalation, while the quantity of Fe is over twice the theoretical value, indicating that not all Fe is inserted in the Pc cavity, as was also observed in XRD through the presence of Fe_2O_3 secondary product.

3.5. OER properties

To validate the electrocatalytic application of the COFs in hand, we next investigated their performance in OER. To test the

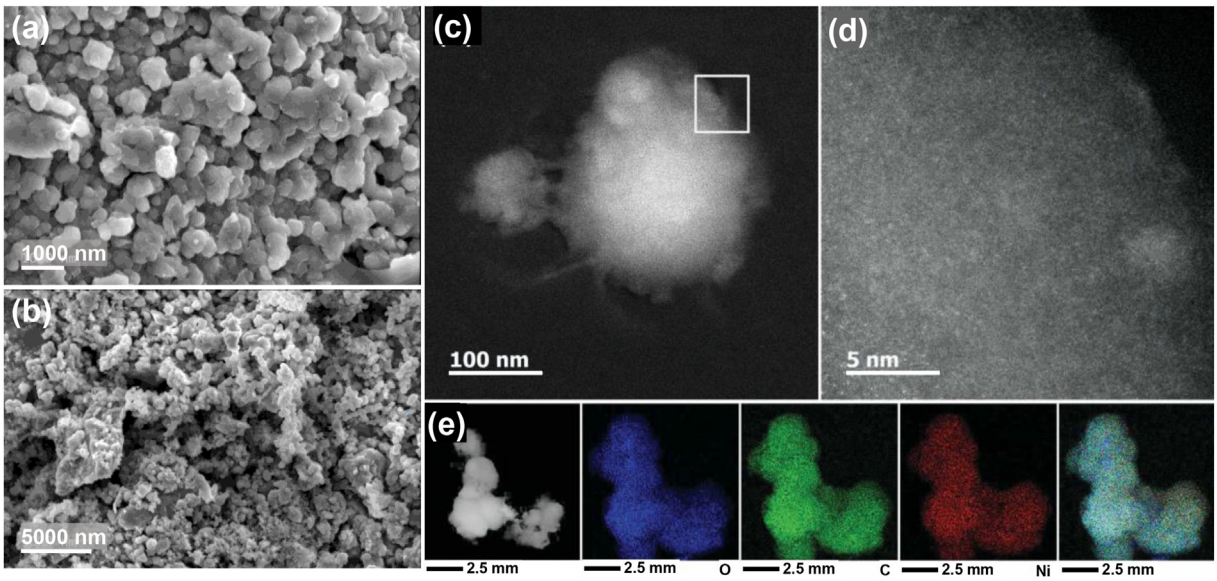

Fig. 2. (a,b) SEM images of NiPcCOF, (c,d) HAADF–STEM images with representative STEM–EDX mappings (e) of O, C, and Ni, and their mixture, indicating a homogeneous distribution of all the elements through the sample.

electrocatalytic activity of the prepared materials for water oxidation under alkaline conditions, the as-synthesized COFs were formulated as inks in ethanol containing conductive Nafion ionomer as binder, and the ink was deposited onto Ni foam current collector.

Notably, the COFs were found to demonstrate the best OER properties at 3 mg cm^{-2} mass loading per geometrical area (Fig. S21). It was also found that prolonged activation via cyclic voltammetry (CV) for about 700 cycles was required to achieve steady state conditions (Fig. S22), after which the materials exhibited constant OER performance.

Fig. 3 and Table S4 summarize the electrochemical water oxidation properties in purified Ar-saturated 1.0 M NaOH of the prepared COF materials supported on Ni foam, as well as that of pure Ni foam. NiPcCOF showed the best results with current densities j of 10, 50, and 100 mA cm^{-2} reached at overpotentials η of around 410 (η_{10}), 460 (η_{50}), and 510 (η_{100}) mV, respectively. H_2NiPcCOF, H_2NiFePcCOF, and H_2FePcCOF were slightly less efficient OER electrocatalysts with η_{10} of ≈430 mV, whereas metal-free H_2PcCOF exhibited similar low performance as Ni foam. As seen in Fig. 3b, the Tafel slopes of metallated COFs are much smaller (b = 62 mV/dec for H_2FePcCOF, b = 68 mV/dec for H_2NiPcCOF, b = 75 mV/dec for NiPcCOF, and b = 78 mV/dec for H_2NiFePcCOF) compared to those of H_2PcCOF (b = 121 mV/dec) and Ni foam (b = 127 mV/dec), indicating faster OER kinetics over these materials.

Electrochemical impedance spectroscopy (EIS) experiments were carried out on stable electrocatalytic system at η_{10}, as illustrated by the Nyquist plots (Fig. 3c), to gain more insight into the OER kinetics. Equivalent circuit model was used to fit the experimental data (Fig. 3c, inset), consisting of a resistor in series with a combination of a resistor and a constant phase element in parallel. Specifically, resistor R_s is the Ohmic resistance from the electrolyte and all contacts. The time constant R_1–CPE_1 is associated with interfacial resistance from electron transport between the electrocatalyst and the Ni foam current collector, while the time constant R_{ct}–CPE_2 is the charge transfer resistance (R_{ct}) at the catalyst–electrolyte interface, with lower R_{ct} values typically reflecting faster charge transfer kinetics [36]. The analysis of the obtained semi-circles (Fig. 3c) as well as derived fitting parameters (Table S5) reveals fastest charge-transfer kinetics over the anode/electrolyte interface in the case of Ni-foam-supported H_2FePcCOF, as reflected by the smallest R_{ct} = 0.132 Ω, followed by Ni-foam-supported H_2NiPcCOF (R_{ct} = 0.137 Ω), H_2NiFePcCOF (R_{ct} = 1.144 Ω), NiPcCOF (R_{ct} = 2.928 Ω), and H_2PcCOF (R_{ct} = 2.982 Ω).

Having proved high OER activity of the as-synthesized COFs, we then investigated if the COFs can generate stable anodic current during alkaline OER. The anodes were subjected to continuous stability testing by means of chronopotentiometry (CP), where the COFs showed excellent long-term stability in 1 M NaOH electrolyte during the tested 100 h. NiPcCOF afforded steady current density j = 10 mA cm^{-2} at overpotential η_{10} of ≈420 mV (Fig. 3d), not suffering from stability issues. Specifically, the overpotential measured for the Ni foam-supported NiPcCOF anode decreased by merely 0.5% over the course of the 100 h electrolysis experiment. The other studied materials also featured relatively stable performance at overpotential η_{10} of ≈430–440 mV up to 100 h.

In order to gain insight into the chemical stability of our electrocatalyst, NiPcCOF after 100 h stability testing was subjected to characterization. HAADF–STEM images with simultaneously collected STEM–EDX mappings indicated that C, O, and Ni remained homogeneously distributed throughout the material (Fig. S24), with some aggregation of Ni evident, which could stem from potential leaching of Ni from the Pc during prolonged alkaline water oxidation.

4. Discussion

Our synthetic strategy to monometallated Pc COFs involved the synthesis of H_2Pc and NiPc. Although their synthesis is straightforward, the low solubility of the Pcs makes their purification time consuming and involves grinding them to fine powders and repeated solvent washes to ensure pure products and success in subsequent reactions. In addition, to remove unreacted building blocks from the COF pores after the synthesis, repeated washing at elevated temperatures (60–100 °C) is required. In the case of NiPcCOF, the presence of small NiO admixture was observed by XRD analysis (Fig. S3). This might be due to minor leaching of Ni

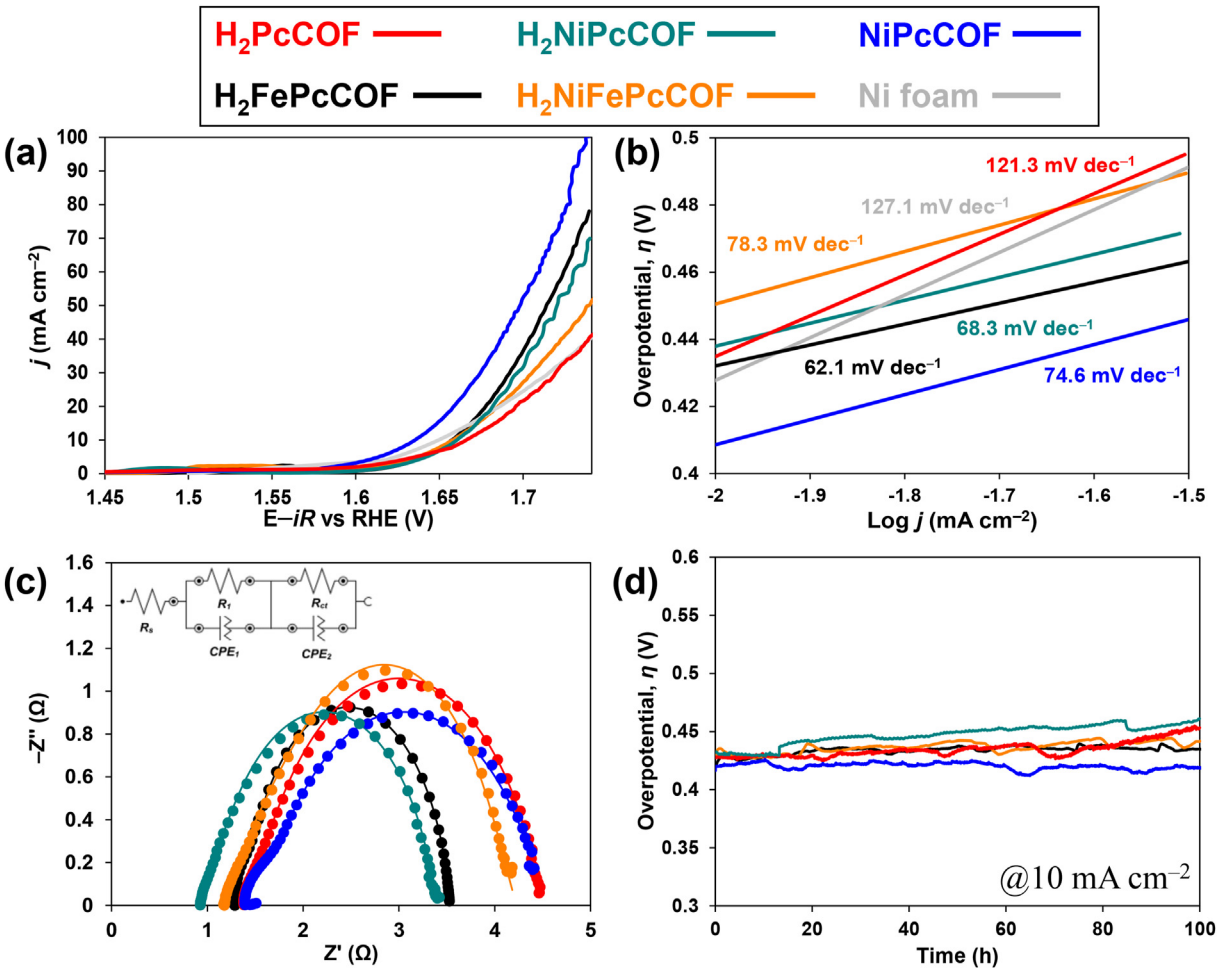

Fig. 3. (a) Anodic polarization curves, (b) Tafel plots, (c) Nyquist plots, and (d) CP profiles at 10 mA cm^{-2} for Ni-foam-supported COFs, all recorded in 1 M NaOH at room temperature with a mass loading of 3 mg cm^{-2}.

from the cavity of Pc during the COF synthesis or the presence of minor Ni impurities in the NiPc building block followed by oxidation. Leaching could be explained by the small size of the Ni ion, which forces the four isoindole groups of the Pc (Scheme 1) to be pulled towards the metal, thus decreasing the cavity diameter of the Pc [37]. This lengthens the C–N–C bonds and decreases the bond angle, causing significant ring deformation, which could facilitate leaching of the metal. At the same time, the XRD patterns of neither H_2NiPcCOF (Fig. S2) nor H_2NiFePcCOF (Fig. S5) showed the presence of NiO side product, which suggests that in the case of NiPcCOF it most likely stems from residual Ni impurities in the building block. In addition, the FTIR spectrum of NiPcCOF clearly showed that the cavities of the Pc are occupied the metal, suggesting that if any leaching occurred, it is rather minor.

To gain access to Fe-bearing COFs with precise control over the metal quantity, the synthesis of FePc building block was attempted using similar procedure as those for NiPc, but despite several efforts the compound could not be isolated in sufficient quality. Therefore, Fe(II) was post-synthetically inserted into the COF structures. The reactions were successful albeit with low yields, which may be due to the exfoliation of the COFs during the post-synthetic reaction. More specifically, Fe(II) insertion is typically carried out using DMF as solvent [29], and some polar solvents, such as DMF, water, and dioxane, may cause layer slipping in 2D COFs depending on the strength of the interlayer interactions of the material [38]. This could also explain the loss of crystallinity of the resultant H_2NiFePcCOF obtained by post-synthetic metalation of H_2NiPcCOF. The XRD analysis of H_2NiFePcCOF (Fig. S5) showed the presence of a small admixture of Fe_2O_3 in the sample, and ICP–OES confirmed that the quantity of Fe in the sample is larger than the theoretical value with all the Pc cavities occupied by the metal. Therefore, the presence of the Fe_2O_3 admixture, which could stem from oxidation of residual $FeCl_2$ remaining in the COF pores after post-synthetic metalation, could also contribute to the loss of crystallinity in this material.

The S_{BET} of all the prepared COFs were in the range of 346–467 m^2/g. Although higher than previously reported for similar Co-containing COF materials [32], the relatively low surface areas and pore size could be an indication of some residual low-solubility oligomers or MPc starting materials remaining in the material despite our intensive washing efforts. In addition, materials formed by polyimide condensation reaction typically suffer from low crystallinity due to the low reversibility of the imide-bond-forming reaction under solvothermal conditions [39], which could further explain the observed textural properties.

Among the COF materials studied, NiPc COF was found to be the most OER active with η_{10} = 410 mV, η_{50} = 460 mV, and η_{100} = 510 mV. However, the material showed a moderate Tafel slope of b = 75 mV/dec, whereas that of H_2FePcCOF was lower with b = 62 mV/dec, despite the higher η_{10} = 430 mV. We postulated that this could be related with the amount of metal in the COF samples, and therefore normalized the electrocatalytic activity data

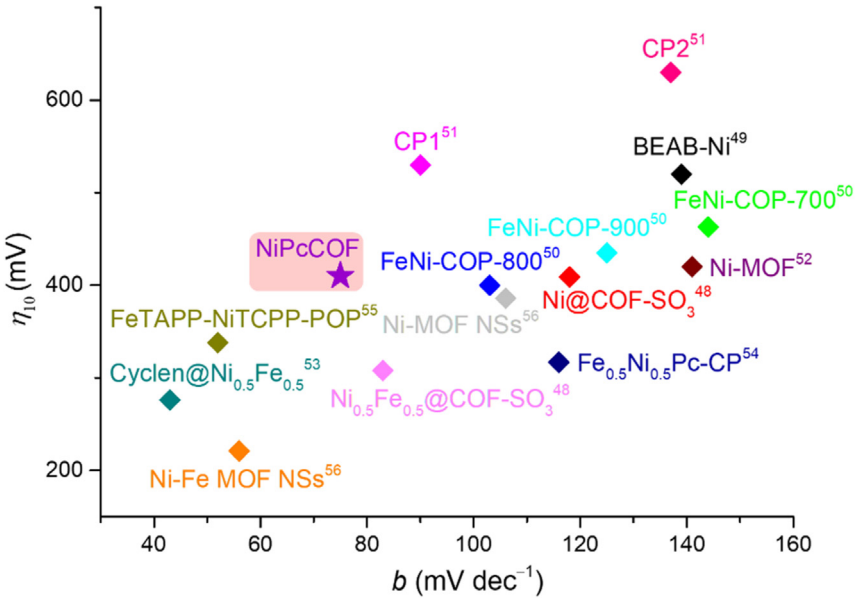

Fig. 4. Comparison of the OER activity of our NiPcCOF with other reported Ni- and Ni/Fe-containing polymers with varying mass loadings.

by the mass of the metal as measured by ICP–OES (Table S6). Indeed, as seen in Fig. S23, the highest mass activity of 1073 mA/mg at $\eta = 500$ mV was found for H_2FePcCOF, followed by H_2NiPcCOF, NiPcCOF, and H_2NiFePcCOF, in good agreement with the Tafel slopes (Fig. 3b) and the Nyquist plots (Fig. 3c).

Of the two possible $4e^-$ transfer pathways for OER, adsorbate evolution mechanism (AEM) and lattice OER (LOER), transition metal Pcs have been suggested to follow the former mechanism [17], whereas the latter has been found for some perovskite catalysts [40–43]. Similarly to metal catalysts, OER in NiPc materials is proposed to proceed through either direct coupling of adjacent Ni–O intermediates or the formation of a Ni–OO species and its subsequent reaction with HO^- [44]. We suggest our NiPcCOF OER electrocatalyst to follow a similar pathway. Such superoxide species have been shown to also play a role in the OER activity of Ni/Fe-based layered double hydroxide and metal–organic framework electrocatalysts [45–47].

In comparison to Ni-containing polymers (Fig. 4) [48–56] our NiPcCOF, with $\eta_{10} \approx 410$ mV and $b = 75$ mV/dec, features catalytic activity among the best of those previously reported for alkaline OER. Annealed bimetallic Pc-based covalent organic polymer FeNi–COP–800, with 0.62% of Fe and 0.47% of Ni, exhibited OER activity of $\eta_{10} \approx 400$ mV and $b = 103$ mV/dec [50]. Porphyrin-based bimetallic FeTAPP–NiTCPP–POP, with 2.8% of Fe and 2.5% of Ni, showed $\eta_{10} \approx 338$ mV and a shallow $b = 52$ mV/dec, whereas the monometallic NiTAPP–NiTCPP–POP (5.8% of Ni) and FeTAPP–FeTCPP–POP (7.2% of Fe) showed lower activities with η_{10} of 384 mV and 520 mV and Tafel slopes of 99 mV/dec and 147 mV/dec, respectively [55]. Using a cation-exchange strategy to incorporate metal ions into the COF–SO_3H structure, metal-containing COFs were obtained, with bimetallic $Ni_{0.5}Fe_{0.5}$@COF–SO_3 showing the best performance ($\eta_{10} \approx 308$ mV; $b = 83$ mV/dec) outperforming monometallic Ni@COF–SO_3 ($\eta_{10} \approx 409$ mV; $b = 118$ mV/dec) and Fe@COF–SO_3 ($\eta_{10} \approx 435$ mV; $b = 123$ mV/dec) [48].

In summary, we have demonstrated a strategy to prepare mono- and bi-metallated COFs with different metal loadings with the catalytic metals atomically dispersed throughout the material. Three COFs were prepared from H_2Pc and NiPc in different ratios under solvothermal conditions to give access to COFs with 0%, 2.4%, and 5.1% of Ni. The COFs with 0% and 2.4% of Ni were further modified by post-synthetic metalation to insert Fe(II) inside the H_2Pc cavity. NiPcCOF with 5.1% of Ni showed the best electrocatalytic activity per geometrical area towards OER under alkaline conditions, with $\eta_{10} \approx 410$ mV and $b = 75$ mV/dec being among the best of Ni-containing polymeric materials reported to date. Nevertheless, the highest mass activity with 1073 mA/mg at $\eta = 500$ mV was found for H_2FePcCOF with 2.1% of Fe. The materials also showed excellent stability over 100 h long-term stability test, showing that the presented approach can be employed to gain access to MPc-containing COFs with promising electrocatalytic performance. Moreover, our synthetic strategy also opens the possibility of future exploration of different metal combinations for further optimization of the electrocatalytic activity for different transformations.

Declaration of competing interest

The authors declare that they have no known competing financial interests or personal relationships that could have appeared to influence the work reported in this paper.

Acknowledgements

This project has received funding from the European Union's Horizon 2020 research and innovation programme under the Marie Skłodowska-Curie grant agreement No 844313, as well as from the European Union's Horizon 2020 research and innovation program through the SpinCat project under Grant Agreement No. 964972. A.M.D. is grateful to Xunta de Galicia for the postdoctoral fellowship (ED481B 2019/091). We thank Drs. J. Sousa, R. D'Amato, and I. Oliveira from INL for the help in N_2 physisorption and ICP–OES measurements.

Appendix A. Supplementary data

Supplementary data to this article can be found online at https://doi.org/10.1016/j.mtchem.2022.101032.

References

[1] A. Wang, J. Li, T. Zhang, Nat. Rev. Chem 2 (2018) 65–81.
[2] Y. Wang, H. Su, Y. He, L. Li, S. Zhu, H. Shen, P. Xie, X. Fu, G. Zhou, C. Feng, D. Zhao, F. Xiao, X. Zhu, Y. Zeng, M. Shao, S. Chen, G. Wu, J. Zeng, C. Wang, Chem. Rev. 120 (2020) 12217–12314.
[3] D.-H. Yang, Y. Tao, X. Ding, B.-H. Han, Chem. Soc. Rev. 51 (2022) 761–791.
[4] J. Wang, Z. Zhang, S. Qi, Y. Fan, Y. Yang, W. Li, M. Zhao, J. Mater. Chem. A 9 (2021) 19949–19957.
[5] D.G. Wang, T. Qiu, W. Guo, Z. Liang, H. Tabassum, D. Xia, R. Zou, Energy Environ. Sci. 14 (2021) 688–728.
[6] X. Zhao, P. Pachfule, A. Thomas, Chem. Soc. Rev. 50 (2021) 6871–6913.
[7] X. Cui, L. Gao, R. Ma, Z. Wei, C.-H. Lu, Z. Li, Y. Yang, J. Mater. Chem. A 9 (2021) 20985–21004.
[8] J. Wang, J. Wang, S. Qi, M. Zhao, J. Phys. Chem. C 124 (2020) 17675–17683.
[9] M. Lu, M. Zhang, C.G. Liu, J. Liu, L.-J. Shang, M. Wang, J.-N. Chang, S.-L. Li, Y.-Q. Lan, Angew. Chem., Int. Ed. 60 (2021) 4864–4871.
[10] H.B. Aiyappa, J. Thote, D.B. Shinde, R. Banerjee, S. Kurungot, Chem. Mater. 28 (2016) 4375–4379.
[11] L.-L. Wang, W.-D. Zhang, T. Li, X. Yan, J. Gao, Y.-X. Chen, Y.-X. Shi, Z.-G. Gu, Chem. Commun. 57 (2021) 13162–13165.
[12] J.-Y. Yue, Y.-T. Wang, X. Wu, P. Yang, Y. Ma, X.-H. Liu, B. Tang, Chem. Commun. 57 (2021) 12619–12622.
[13] M. Urbani, M.-E. Ragoussi, M.K. Nazeeruddin, T. Torres, Coord. Chem. Rev. 381 (2019) 1–64.
[14] A. Kumar, V. Kumar Vashistha, D. Kumar Das, Coord. Chem. Rev. 431 (2021) 213678.
[15] A. Valverde-González, L.Z. Guan, M.L. Ferrer, M. Iglesias, E.M. Maya, ACS Appl. Mater. Interfaces 12 (2020) 32681–32688.
[16] S. Hadimane, S. Aralekallu, K. Prabhu CP, M. Hojamberdiev, L.K. Sannegowda, ACS Appl. Energy Mater. 4 (2021) 10826–10834.
[17] S. Yang, Y. Yu, X. Gao, Z. Zhang, F. Wang, Chem. Soc. Rev. 50 (2021) 12985–13011.
[18] H. Zhong, M. Wang, M. Ghorbani-Asl, J. Zhang, K.H. Ly, Z. Liao, G. Chen, Y. Wei, B.P. Biswal, E. Zschech, I.M. Weidinger, A. V Krasheninnikov, R. Dong, X. Feng, J. Am. Chem. Soc. 143 (2021) 19992–20000.
[19] Y. Liu, X. Yue, K. Li, J. Qiao, D.P. Wilkinson, J. Zhang, Coord. Chem. Rev. 315 (2016) 153–177.
[20] M.-D. Zhang, D.-H. Si, J.-D. Yi, Q. Yin, Y.-B. Huang, R. Cao, Science China Chemistry 64 (2021) 1332–1339.
[21] Y. Yue, P. Cai, K. Xu, H. Li, H. Chen, H.-C. Zhou, N. Huang, J. Am. Chem. Soc. 143 (2021) 18052–18060.
[22] M. Jiang, L. Han, P. Peng, Y. Hu, Y. Xiong, C. Mi, Z. Tie, Z. Xiang, Z. Jin, Nano Lett. 22 (2022) 372–379.
[23] S. Divanis, T. Kutlusoy, I.M. Ingmer Boye, I.C. Man, J. Rossmeisl, Chem. Sci. 11 (2020) 2943–2950.
[24] Q. Kang, D. Lai, W. Tang, Q. Lu, F. Gao, Chem. Sci. 12 (2021) 3818–3835.
[25] X. Wang, Z.-F. Cai, D. Wang, L.-J. Wan, J. Am. Chem. Soc. 141 (2019) 7665–7669.
[26] Y.J. Kim, A. Lim, J.M. Kim, D. Lim, K.H. Chae, E.N. Cho, H.J. Han, K.U. Jeon, M. Kim, G.R: Lee, H.S. Ahn, H.S. Park, H. Kim, J.Y. Kim, Y.S. Jung, Nat. Commun. 11 (2020) 4921.
[27] L.M. Salonen, D.Y. Petrovykh, Yu.V. Kolen'ko, Mater. Today Sustain. 11–12 (2021) 100060.
[28] Z. Chen, W. Wei, B.-J. Ni, Curr. Opin. Green Sustain. Chem. 27 (2021) 100398.
[29] D. Wöhrle, G. Meyer, B. Wahl, Makromol. Chem. 181 (1980) 2127–2135.
[30] N. Kobayashi, T. Ohya, M. Sato, S. Nakajima, Inorg. Chem. 32 (1993) 1803–1808.
[31] M. Bai, R. Song, Y. Zhang, S. Han, X. Song, F. Meng, Inorg. Chem. Commun. 28 (2013) 99–103.
[32] B. Han, X. Ding, B. Yu, H. Wu, W. Zhou, W. Liu, C. Wei, B. Chen, D. Qi, H. Wang, K. Wang, Y. Chen, B. Chen, J. Jiang, J. Am. Chem. Soc. 143 (2021) 7104–7113.
[33] J. Maschita, T. Banerjee, B.V. Lotsch, Chem. Mater. 34 (2022) 2249–2258.
[34] Z. Song, H. Zhan, Y. Zhou, Angew. Chem. Int. Ed. 49 (2010) 8444–8448.
[35] S. Wei, H. Zou, W. Rong, F. Zhang, Y. Ji, L. Duan, Appl. Catal. B Environ. 284 (2021) 119739.
[36] N Bonanos, B.C.H. Steele, E.P. Butler, J.R. Macdonald, W.B. Johnson, W.L. Worrell, G.A. Niklasson, S Malmgren, M Strømme, S.K. Sundaram, M.C.H. McKubre, D.D. Macdonald, G.R. Engelhardt, E Barsoukov, B.E. Conway, W.G. Pell, N. Wagner, C.M. Roland, R.S. Eisenberg, Applications of Impedance Spectroscopy, in: E. Barsoukov, J.R. Macdonald (Eds.), Impedance Spectroscopy: Theory, Experiment, and Applications, third ed., John Wiley & Sons, Ltd., 2018, p. 175.
[37] D.R. Tackley, G. Dent, W.E. Smith, Phys. Chem. Chem. Phys. 3 (2001) 1419–1426.
[38] D.N. Bunck, W.R. Dichtel, J. Am. Chem. Soc. 135 (2013) 14952–14955.
[39] J. Maschita, T. Banerjee, G. Savasci, F. Haase, C. Ochsenfeld, B.V. Lotsch, Angew. Chem. Int. Ed. 59 (2020) 15750–15758.
[40] X. Cheng, E. Fabbri, M. Nachtegaal, I.E. Castelli, M. El Kazzi, R. Haumont, N. Marzari, T.J. Schmidt, Chem. Mater. 27 (2015) 7662–7672.
[41] A. Grimaud, O. Diaz-Morales, B. Han, W.T. Hong, Y.-L. Lee, L. Giordano, K.A. Stoerzinger, M.T.M. Koper, Y. Shao-Horn, Nat. Chem. 9 (2017) 457–465.
[42] S. Hong, A.M. Diez, A.N. Adeyemi, J.P.S. Sousa, L.M. Salonen, O.I. Lebedev, Yu.V. Kolen'ko, J.V. Zaikina, ACS Appl. Mater. Interfaces 14 (2022) 23277–23284.
[43] J.-W. Zhao, C.-F. Li, Z.-X. Shi, J.-L. Guan, G.-R. Li, Research (2020) 6961578.
[44] N. Alzate-Carvajal, L.M. Bolivar-Pineda, V. Meza-Laguna, V.A. Basiuk, E.V. Basiuk, E.A. Baranova, ChemElectroChem 7 (2020) 428–436.
[45] C.-F. Li, L.-J. Xie, J.-W. Zhao, L.-F. Gu, J.-Q. Wu, G.-R. Li, Appl. Catal. B Environ. 306 (2022) 121097.
[46] C.-F. Li, L.-J. Xie, J.-W. Zhao, L.-F. Gu, H.-B. Tang, L. Zheng, G.-R. Li, Angew. Chem. Int. Ed. 61 (2022) e202116934.
[47] C.-F. Li, J.-W. Zhao, L.-J. Xie, J.-Q. Wu, Q. Ren, Y. Wang, G.-R. Li, Angew. Chem. Int. Ed. 60 (2021) 18129–18137.
[48] Z. Gao, L.L. Gong, X.Q. He, X.M. Su, L.H. Xiao, F. Luo, Inorg. Chem. 59 (2020) 4995–5003.
[49] T. Li, C. Atish, K. Silambarasan, X. Liu, A.P. O'Mullane, Electrochim. Acta 362 (2020) 137212.
[50] Z. Liao, Y. Wang, Q. Wang, Y. Cheng, Z. Xiang, Appl. Catal. B Environ. 243 (2019) 204–211.
[51] T. Kumar, A. Karmakar, A. Halder, R.R. Koner, Energy Fuels 36 (2022) 2722–2730.
[52] A. Xie, J. Du, F. Tao, Y. Tao, Z. Xiong, S. Luo, X. Li, C. Yao, Electrochim. Acta 305 (2019) 338–348.
[53] X. Feng, Z. Gao, L. Xiao, Z. Lai, F. Luo, Inorg. Chem. Front. 7 (2020) 3925–3931.
[54] D. Qi, X. Chen, W. Liu, C. Liu, W. Liu, K. Wang, J. Jiang, Inorg. Chem. Front. 7 (2020) 642–646.
[55] J. Meng, Z. Xu, H. Li, D.J. Young, C. Hu, Y. Yang, ChemCatChem 13 (2021) 1396–1402.
[56] F.-L. Li, P. Wang, X. Huang, D.J. Young, H.-F. Wang, P. Braunstein, J.-P. Lang, Angew. Chem. Int. Ed. 58 (2019) 7051–7056.